

COVER SHEET

Title: **Particle Modeling for Blasting Simulations**

Authors: G. Wang
A. Al-Ostaz
A.H.-D. Cheng
P.R. Mantena

ABSTRACT

Particle modeling (PM) is an innovative particulate dynamics based modeling approach. In brief, PM is a numerical technique similar to the molecular dynamic (MD) simulation; but rather than simulating actual atoms, it is based on lumped mass particles distributed on a grid to allow macro scale modeling. The PM utilizes an equivalent Lennard-Jones, polynomial or quadratic potential to model the nonlinear or linear constitutive law at the continuum, macroscopic level. The mass has inertia that obeys Newton's second law of motion. It is a Lagrangian model that keeps track of particle location and velocity.

As is known, dynamic fragmentation dominantly occurs in a blasting process that becomes an overwhelming difficulty to any continuum-based approaches. However, the basic treatment of PM, in which fracture is created when a bond (spring) is broken by translational force, provides PM a unique power to be able to quite easily overcome a "discontinuity of material" problem. This paper will present the PM and its application for blasting simulations.

Keywords: particle modeling, lattice model, fracture mechanics, blast.

G. Wang (corresponding author), Civil Engineering Department, University of Mississippi, Oxford, MS, 38677-1848, USA.

A. Al-Ostaz, Civil Engineering Department, University of Mississippi, Oxford, MS, 38677-1848, USA.

A.H.-D. Cheng, Civil Engineering Department, University of Mississippi, Oxford, MS, 38677-1848, USA.

P.R. Mantena, Mechanical Engineering Department, University of Mississippi, Oxford, MS, 38677-1848, USA.

INTRODUCTION

The prompt development of modern computer technology and computational methods enables scientists, more easily than ever before, to numerically examine the nature of materials, to verify or modify the existing theories, and even to discover new phenomena. Blasting simulation of materials also greatly benefits from this advancement.

Blasting of materials is an extremely challenging topic of dynamic fracture mechanics. A blasting process itself is an exceedingly complex, multi-scale physical phenomenon with dynamic fragmentation dominantly occurring that becomes an overwhelming difficulty to numerical approaches. Hence, an ideal solver for blasting simulations is required to be able to handle all the above-mentioned factors, especially to deal with the evolving discontinuity of material.

An all-round search to the existing optional modeling techniques reveals that the modern numerical methods for blasting simulations at macroscopic level can be generally classified into two categories of approaches. One is continuum mechanics based and the other is discrete element based. Examining the state-of-the-art of the research, we conclude that the continuum mechanics based approaches, such as the finite element method (FEM), have difficulty in solving dynamic fracture problems, particularly in dealing with the simulation of the collapse of structure and its fragmentation under extreme loading conditions. For this reason, another domain of alternative modeling approach—the discrete element based models, has become more and more popular.

Discrete element models share a common concept of “discrete material”, which can still be further classified into two sub-categories. The first one is classified as a discrete element method, in which the physical size and shape of each element is considered in the computation, such as the applied element method (AEM) [1], and particle finite element method (PFEM) [2] - another particle-related model. In practice, this type of models is complex and difficult to be implemented. For instance, AEM is laborious in keeping track of the instantaneous contact positions and the evolving geometry of all elements for a proper updating of the dynamic bonds; PFEM is expensive in remeshing and redefining boundaries at each time step.

The second branch is named particle (or particulate) dynamics method, in which the physical size and shape of each discrete cell is not explicitly considered in the computation. Consequently, each cell is treated as a particle, with the equivalent mass lumped at its center. Smoothed particle hydrodynamics (SPH) [3], and particle modeling (PM) are currently the mainly two popular particulate based models. SPH adopts a kernel probability density function to define for each particle a reaction domain at each time step, in terms of a particle number density; it is therefore highly expensive in computation. In contrast, PM is rather simple in theory and easy for implementation; hence, it is attracting increasing interest, despite a good number of SPH codes.

PM is a numerical technique similar to the molecular dynamic (MD) simulation; but rather than simulating actual atoms, it is based on lumped mass particles distributed on a grid to allow macro scale modeling. The PM utilizes an equivalent Lennard-Jones, polynomial or quadratic potential to model the nonlinear or linear constitutive law at the continuum, macroscopic level. The mass has inertia that obeys Newton’s second law of motion. It is a Lagrangian model that keeps track of particle location and velocity. This method was originally proposed by Greenspan [4, 5]. However, as no direct link with the

material properties was attempted by Greenspan, Greenspan's PM method remains a conceptual model without a demonstrated success in fracture modeling.

Wang and Ostoja-Starzewski [6] developed a newly modified PM with a conventional linkage pattern as shown in Figure 1. In this new PM, equivalent material properties are formulated using four physical conditions to determine continuum-level Young's modulus and tensile strength, while maintaining the conservation of mass and energy of the particle system, and satisfying the interaction laws among all the particles. The theoretical foundations of the current PM can be outlined in the following four aspects:

- (a) Derivation is based on equivalence/equality of mass, energy, elastic moduli and tensile strengths between both atomic and quasi-particle systems.
- (b) Derivation is carried out in the setting of a 3-D *face-centered cubic (f.c.c)* lattice network (Figure 2) for both atomic and quasi-particle structures.
- (c) Either Lennard-Jones, polynomial or quadratic potentials can be employed for nonlinear or linear axial linkage.
- (d) In principle, it can be applied for various length scale problems of solids.

In the coming sections, first we will introduce the theory of PM and its current success in applications; then a preliminary blasting study of PM will be reported; and finally, in the conclusion part, an outlook of future-going work is to be outlined.

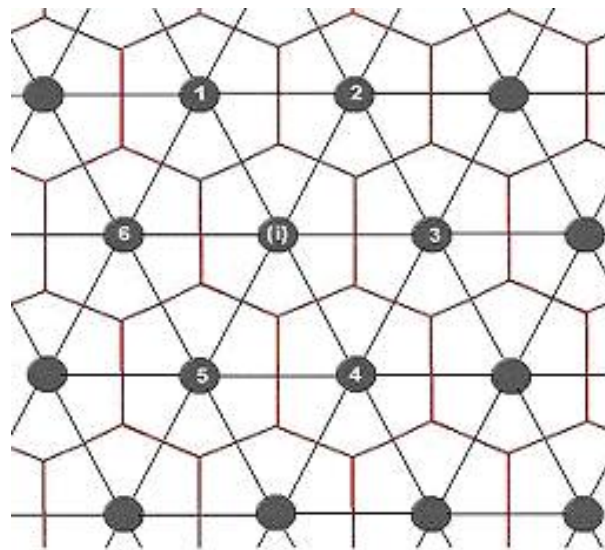


Figure 1 Lattice structure in PM.

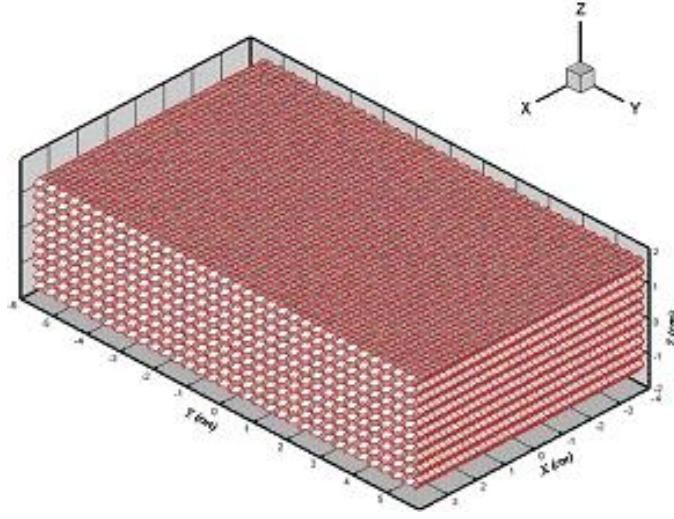


Figure 2 Meshing system for a 3D material body.

METHODOLOGY OF PM

In particle modeling (PM), the nonlinear interaction force is considered between nearest-neighbor (quasi-) particles and assumed to be of the same form as in MD:

$$F = -\frac{G}{r^p} + \frac{H}{r^q} \quad (1)$$

Here G , H , p and q are positive constants, and $q > p \geq 1$ to obtain the repulsive effect that is necessarily (much) stronger than the attractive one, r being the distance between two particles.

Ashby & Jones [7] presented a simple method to evaluate continuum-type Young's modulus E and tensile stress $\sigma(r)$ of the material from $F(r)$, namely

$$E = \frac{S_0}{r_0} \quad (2)$$

and

$$\sigma(r) = NF(r) \quad (3)$$

where $S_0 = (dF / dr)_{r=r_0}$, and r_0 is the equilibrium spacing between contiguous particles. N is the number of bonds/unit area, equal to $1/r_0^2$. Tensile strength, σ_{TS} , results when $dF(r_d)/dr = 0$, that yields,

$$\sigma_{TS} = NF(r_d) \quad (4)$$

Just as in MD, the non-linear dynamical equation of motion for each particle P_i of the PM system is given by

$$m_i \frac{d^2 \vec{r}_i}{dt^2} = \sum \left[\left(-\frac{G_i}{r_{ij}^p} + \frac{H_i}{r_{ij}^q} \right) \frac{\vec{r}_{ji}}{r_{ij}} \right], \quad i \neq j \quad (5)$$

where m_i and \vec{r}_{ji} are mass of P_i and the vector from P_j to P_i . Note that if an equilateral triangular lattice structure is adopted in 2-D, the resulting Poisson ratio equals 1/4 (or 1/3) when a 3-D (respectively, plane) elasticity formulation is adopted [8, 9].

The derivation of four parameters in Eq. (1) from MD structures is conducted on a cubic body with volume $V (= A \times B \times C)$, in Figure 2. A face-centered cubic (*f.c.c*) lattice for both atomic and quasi-particle structures is chosen. If p , q and r_0 are given, then, by conditions of mass and energy conservation, G and H can be derived. Consequently, Young's modulus is evaluated by Eq. (2) and tensile strength by Eq. (4). To represent an expected material property, we would have to do many sets of testing until a unique (p, q) is found to match both Young's modulus and tensile strength of the material. The complete derivation process is described below.

First, for the atomic structure (MD model), we have: interaction potential energy (*ergs*):

$$\varphi_a = \left(\frac{G_a r^{1-p_a}}{1-p_a} + \frac{H_a r^{1-q_a}}{1-q_a} \right) \times 10^{-8} \quad (6)$$

Young's modulus (*GPa*) is obtained from Eq. (2) and tensile strength (*MPa*) from Eq. (4).

Total number of atoms in $A \times B \times C$ cubic material body:

$$N^* = \left(\frac{A \times 10^8}{r_a} + 1 \right) \times \left(\frac{B \times 10^8}{r_a \sin 60^\circ} + 1 \right) \times \left(\frac{C \times 10^8}{r_a \sqrt{6}/3} + 1 \right) \quad (7)$$

In Eqs. (6) and (7), r_a is equilibrium position of the simulated material in atomic structure, and p_a , q_a are the exponential parameters in atomic structure. Note that, for a Lennard-Jones interaction case, $p_a = 7$ and $q_a = 13$.

Next, for the quasi-particle structure (PM model), we have interaction force (*dynes*) as in Eq. (1).

Interaction potential energy (*ergs*):

$$\phi = \frac{G r^{1-p}}{1-p} + \frac{H r^{1-q}}{1-q}, \text{ for } p > 1; \phi = G \ln r + \frac{H r^{1-q}}{1-q}, \text{ for } p = 1 \quad (8)$$

total number of quasi-particles in PM system:

$$N = i_{\max} \times j_{\max} \times k_{\max} \quad (9)$$

We now postulate the equivalence of MD and PM models. From the mass conservation, we calculate the mass of each quasi-particle m based on atomic mass m_a :

$$m = N^* \times m_a / N \quad (10)$$

From the energy conservation, we have:

$$(N \times \phi)_{r=r_0} = (N^* \times \phi_a)_{r=r_a} \quad (11)$$

under the requirement:

$$F(r_0) = 0 \quad (12)$$

From equations (11), (12), we now derive Young's modulus E :
for $p = 1$:

$$G = Hr_o^{1-q}, \quad H = \frac{(N^* \times \phi_a)_{r=r_a} (1-q)}{N(1-q)r_o^{1-q} \ln r_o - r_o^{1-q}}, \quad E = -Gr_o^{-3} + qHr_o^{-q-2} \quad (13)$$

for $p > 1$:

$$G = Hr_o^{1-q}, \quad H = \frac{(N^* \times \phi_a)_{r=r_a} (1-p)(1-q)}{N(p-q)} r_o^{q-1}, \quad E = -pGr_o^{-p-2} + qHr_o^{-q-2} \quad (14)$$

Similarly, tensile strength can be obtained under $dF(r_d)/dr = 0$. Evidently, the four parameters (p, q), r_0 and V affect E and σ_{TS} .

We have established the equations for G, H, p and q , and carried out a parametric study to find the differing effects on p, q, V and r_0 [6]. Herein, we summarize the obtained rules as follows:

- (i) The larger the values of (p, q) are adopted, the larger is E generated. This is typically associated with the material becoming more brittle than ductile, albeit there is a range of toughness to choose from. Also, with E going up, there is a fragmentation into a larger number of pieces.
- (ii) In the case of $p = 1$, the larger r_0 spacing is adopted, the higher is Young's modulus of the PM material. On the contrary, in the special case of $p \neq 1$, there is an opposite trend. In any case, this increase or decrease does not change very much.
- (iii) In the case of $p \neq 1$, while keeping the volume fixed, an increase of r_0 produces a decrease of Young's modulus. The situation is again opposite in the case of $p = 1$.
- (iv) A uniform augmentation of volume V by dilation in all three coordinate directions (xyz) , at any (p, q) combination, results in Young's modulus increasing first strongly and then leveling off.

For brittle materials, a general format of linear dynamical equation is often employed [10],

$$F = \begin{cases} -S_0(r - r_0) & \text{for } r_c \leq r \leq r_t \\ 0 & \text{otherwise} \end{cases} \quad (15)$$

with r being the distance between two particles, the stiffness $S_0 = E \bullet r_0$ by Eq. (2), E the Young modulus and r_{\max} the failure displacement of material, r_0 the equilibrium spacing between the contiguous particles.

In Equation (15), r_c and r_t are the fracture positions applied for compression and tension, respectively, which need to be empirically determined.

The leapfrog method, with second-order accuracy, is employed in all PM simulations. The leapfrog formulas relating position, velocity and acceleration for particles P_i ($i = 1, 2, \dots, N$) [4] are

$$\vec{V}_{i,1/2} = \vec{V}_{i,0} + \frac{(\Delta t)}{2} \vec{a}_{i,0} \quad (\text{starter formula}) \quad (16)$$

$$\vec{V}_{i,k+1/2} = \vec{V}_{i,k-1/2} + (\Delta t) \vec{a}_{i,k}, \quad k = 1, 2, 3, \dots \quad (17)$$

$$\vec{r}_{i,k+1} = \vec{r}_{i,k} + (\Delta t) \vec{V}_{i,k+1/2}, \quad k = 0, 1, 2, \dots \quad (18)$$

where $\vec{V}_{i,k}$, $\vec{a}_{i,k}$ and $\vec{r}_{i,k}$ are the velocity, acceleration and position vectors of particle i at time $t_k = k\Delta t$, Δt is the time step. $\vec{V}_{i,k+1/2}$ stands for the velocity of particle i at time $t_k = (k + 1/2)\Delta t$, and so on. Notably, the leapfrog method is of second-order accuracy: $O((\Delta t)^2)$.

The safe time step is after the derivation result by Hockney & Eastwood [11]:

$$\Omega \bullet \Delta t \ll 2, \Omega = \left(\frac{1}{m} \left| \frac{dF}{dr} \right|_{\max} \right)^{1/2} \quad (19)$$

To readily describe the breakage effect on material, we define a concept of fracture density [12]. By this definition, the local fracture density of particle i , $f_{i.den.}$, is equal to the ratio of its current number of broken bonds, N_{b_i} to its original number of bonds, N_{o_i} , i.e.,

$$f_{i.den.} = \frac{N_{b_i}}{N_{o_i}} \quad (20)$$

It is clearly seen that a big $f_{i.den.}$ value indicates a severe failure locally occurring at i .

PM VALIDATION WORK

The first successful application of PM has been achieved for simulation of dynamic fragmentation in an (elastic-brittle) epoxy plate (8.25 cm x 33.02 cm), containing non-uniformly distributed circular holes in tension [13]. As demonstrated in Figure 3(a, b), PM forecasting of the crack pattern agrees well with the associated empirical observation [14].

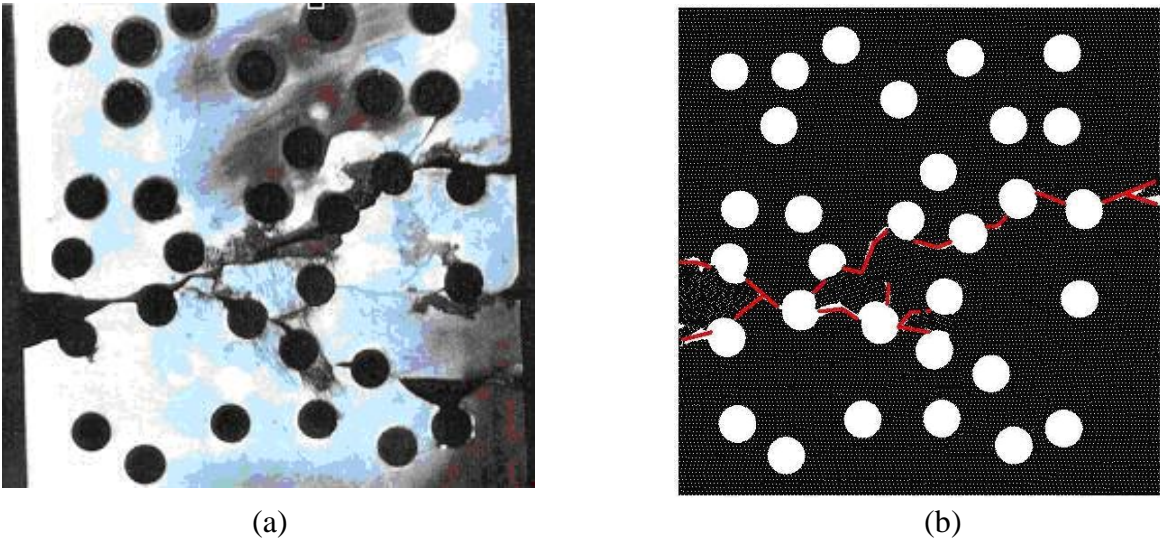
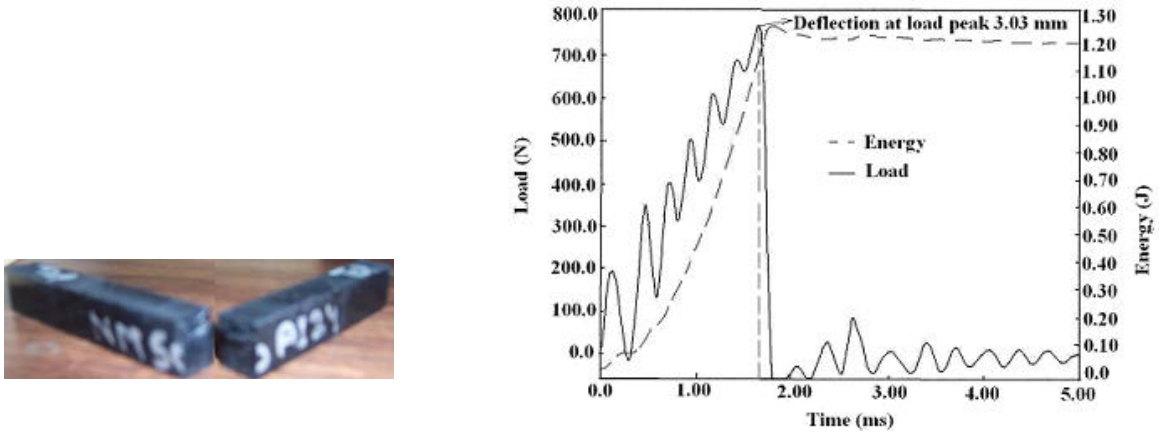
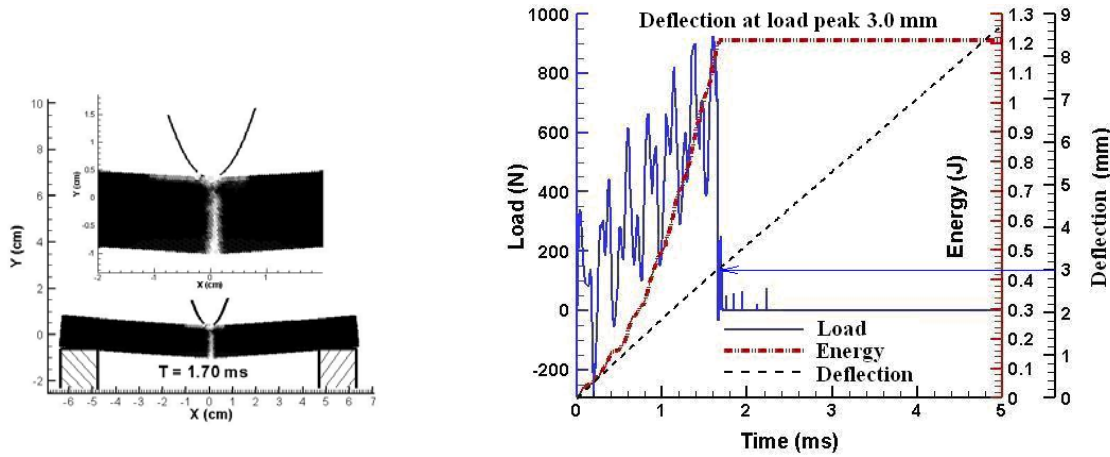


Figure 3 Experimental and modeling results of epoxy in tension, (a) experiment [14], (b) PM simulation [13].

Other two validations of the PM are conducted by simulating the impact of a rigid indenter on polymeric materials (nylon-6, 6 and vinyl ester). Figure 4(a, b) shows the comparison of the experimental result of fracture pattern of nylon-6,6 due to the impact of a rigid indenter [10] while Figure 5(a, b) shows the comparison of the similar impact study of vinyl ester. The associated experiments were conducted at the University of Mississippi.

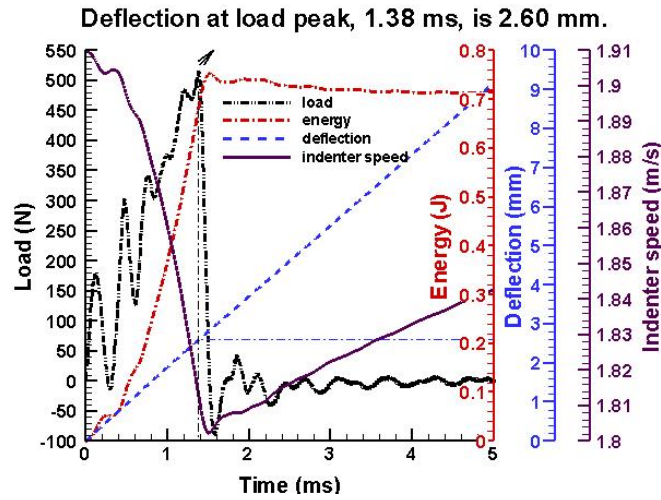


(a) Experimental results

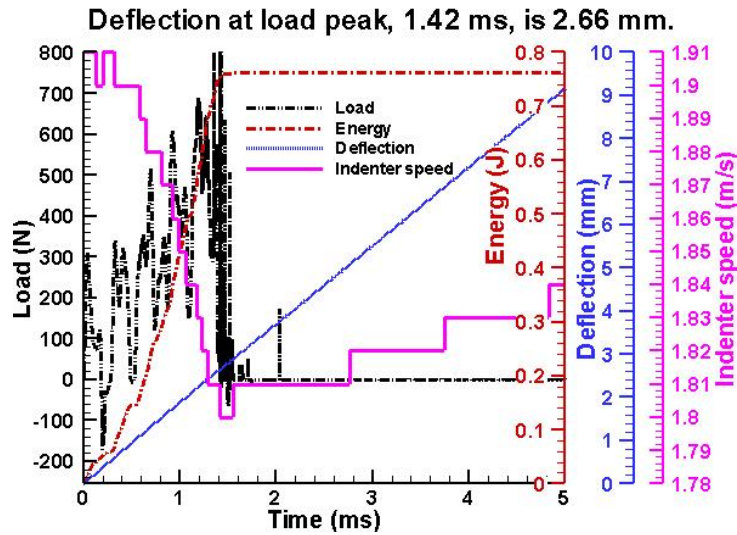


(b) PM results

Figure 4 The study of the failure of nylon-6, 6 due to the impact of a rigid indenter (a) experimental results; (b) PM results. Maximum drop velocity of indenter is 1.87 m/s. [10].



(a) Experimental results



(b) PM results

Figure 5 Comparison of experimental and modeling results of vinyl ester due to the impact of a rigid indenter: load, energy, deflection and indenter speed curves versus time. Maximum drop velocity of indenter is -1.91 m/s . [Experiment conducted at the University of Mississippi].

From Figure 4(a, b), it found that (1) PM modeling crack pattern agrees with the associated observation, and (2) it is seen that measured load peak happens around $t \approx 1.70$ ms, and the measured deflection at the load peak is 3.03 mm, with the total impact energy equal to 1.2 J. The corresponding PM simulated result shows that the load peak happens around $t \approx 1.66$ ms, and the deflection at load peak is 3.0 mm, and the total impact energy calculated is 1.2 J. Although the simulated load profile is not exactly the same as the experiment, we observe similar characteristics, including the fluctuating profile with roughly the same period. The simulated peak load is also reasonable close to the experimental value. Hence we conclude that the PM simulation compares favorably with the experimental measurements.

From Figure 5(a, b), it is seen that measured load peak happens around $t \approx 1.38$ ms, and the measured deflection at the load peak is 2.60 mm, with the total impact energy equal to 0.7 J. The corresponding PM simulated result shows that the load peak happens around $t \approx 1.42$ ms, and the deflection at load peak is 2.66 mm, and the total impact energy calculated is 0.76 J. Similarly to Figure 4(a, b), although the simulated load profile is not exactly the same as the experiment, we observe similar characteristics, including the fluctuating profile with roughly the same period. The simulated peak load is also reasonable close to the experimental value. Hence we conclude that the PM simulation compares favorably with the experimental measurements.

After the confidence with the model is gained, next, some preliminary blasting simulations of PM will be presented.

BLASTING SIMULATIONS OF PM

In this section, PM blasting simulations of a wall will be briefly presented, with and without a retrofitting treatment. The purpose of this study is first to demonstrate the effectively protective effect of the employment of a retrofitting enforcement. Then, an idea to fabricate an optimal reinforcement is preliminary pursued.

The wall is made of concrete and the retrofitting structure is a three-layered composition of different materials as shown in Figure 6. The top and bottom ends are fully fixed.

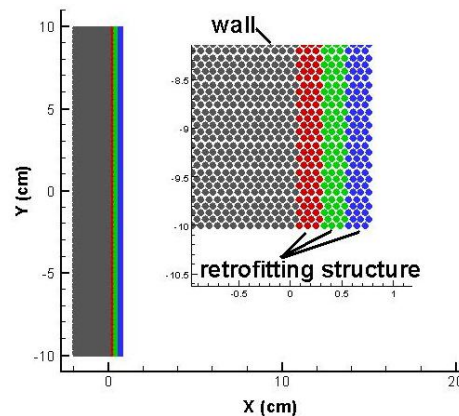


Figure 6 A concrete wall with a three-layered retrofitting structure.

Eq. (15) is used to define dynamics of the concrete wall when subject to a blasting load; different (p, q) is assigned into Eq. (1) to define a different material composition of the layered reinforcement structure.

The detonation is place on the left side of the structure system shown in Figure 6. The dynamic pressure vs. time for a blasting process follows Eq. (21),

$$P(t) = P_0 \bullet \left(1 - \frac{t}{t_d}\right) \bullet e^{-\frac{t}{t_d}} \quad (21)$$

where P_0 is the pressure peak, and t_d is the duration of blasting. In the present simulations, $P_0 = 4 \text{ Kpsi}$ and $t_d = 25 \text{ ms}$.

7(a, b) displays the PM blasting results of a wall with and without a retrofitting treatment at $t = 0.296 \text{ ms}$. In the latter case, the (p, q) values for the three-layered material structure are, respectively, assigned as $(3, 5)$, $(5, 10)$ and $(7, 14)$. According to [6], the resultant material property of using different (p, q) in Eq. (1) behaves like that, the larger the value of (p, q) is adopted, the larger is E generated. This is typically associated with the material becoming more brittle than ductile, albeit there is a range of toughness to choose from. Also, with E going up, there is a fragmentation into a larger number of pieces.

From Fig. 7(a) it is found that for the case without the retrofitting enforcement attached to infrastructure, debris flow of the material will fly into the area behind the wall after the structure is fractured, and consequently can cause severe damage to the creatures wherein. In contrast, for the case with the retrofitting consideration, due to the resistance from the enforcement of the layered material, there are no material fragments intruding into the area behind the wall, as shown in Fig. 7(b); hence, people and facilities in the area will be well protected.

Figure 8(a, b) records the time-dependent displacement values of the right mid-points associated with the two above-shown cases in Figure 7(a, b). It is clearly seen that the maximum displacement value for the case with a retrofitting consideration is much smaller than the case without reinforcement. This demonstrates the necessity and importance of the adoption of a retrofitting structure attached to the infrastructure.

Figure 9 shows the time-dependent displacement result of the right mid-point associated with using $(p, q) = (7, 14)$, $(3, 5)$ and $(5, 10)$ for the three-layered material structure.

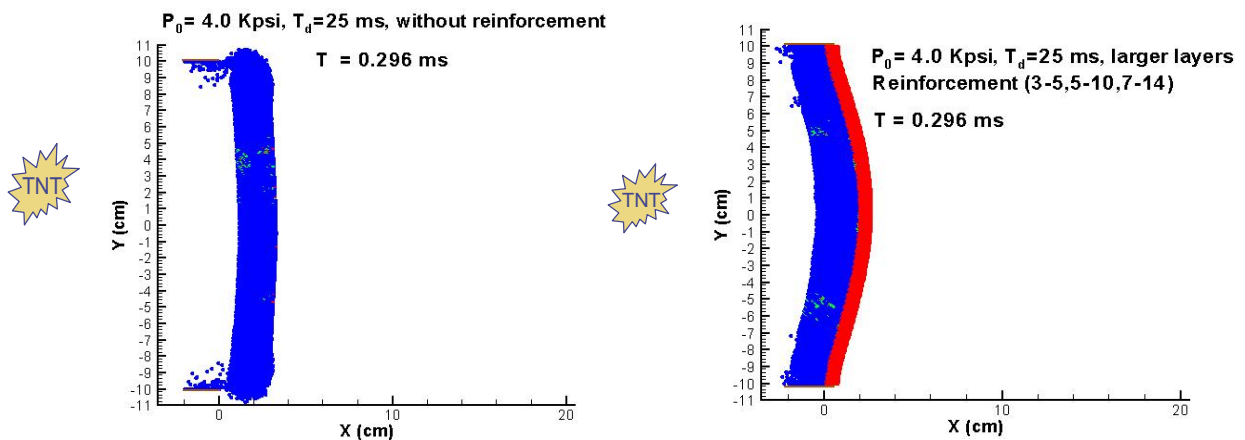
Compared with Figure 8(b) and 9, we observe that the maximum displacement values for the two different (p, q) settings are different. Although only limited investigation study is accomplished at present stage, from the above-obtained information, we can still conclude that an optimal composition of (p, q) for the layered structure, in equivalence of different materials, exists that can greatly provide a maximum protective result to the wall when subject to a blasting event. We will report the associated research progress in our future publications.

CONCLUSIONS

In the present paper, a particulate dynamics based method, particle modeling (PM), is introduced. Then, some preliminary blasting simulations of PM are reported. For instance, the cases of wall with- and without retrofitting layered structure are simulated when subject to a dynamic blasting load. It is found that the retrofitting layered structure can greatly restrain the distance of the debris of infrastructure from intruding the living areas behind after it fails in a blasting process. Thus, the personnel and facilities in the building can be well protected. Meanwhile, different combination of materials is preliminarily attempted to fabricating an optimal reinforcement structure to gain an optimal protective effect.

Our future-going research work of PM blasting study can be outlined as follows:

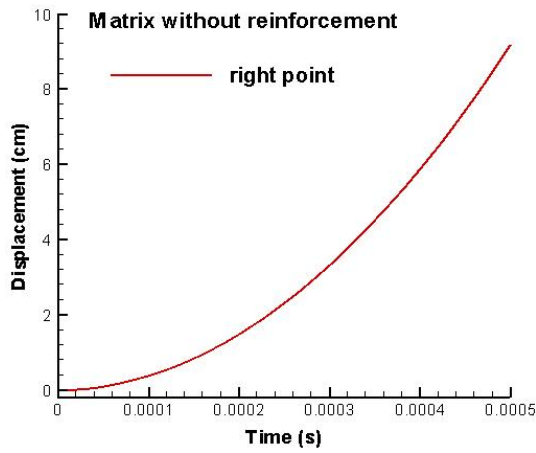
- (1) Validation of the PM blasting model with real tests.
- (2) Conduction of serial simulations accounting for different combination of materials to fabricate the layered retrofitting structure to find out an optimal protective solution to an infrastructure system.



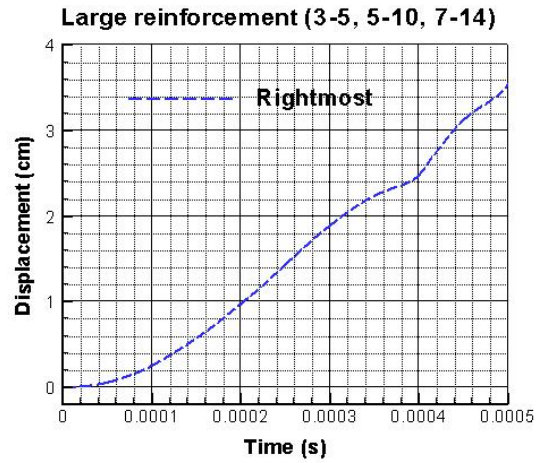
(a) homogenous material

(b) retrofitting material structure

Figure 7 Examples of PM simulations of blasting (a) homogeneous material, (b) retrofitting material structure with $(p, q) = (3, 5), (5, 10)$ and $(7, 14)$. $t = 0.296\text{ms}$.



(a) Without retrofitting protection.



(b) With retrofitting protection.

Figure 8 Time-dependent displacement record (a) homogeneous material, (b) retrofitting material structure with $(p, q) = (3, 5), (5, 10)$ and $(7, 14)$.

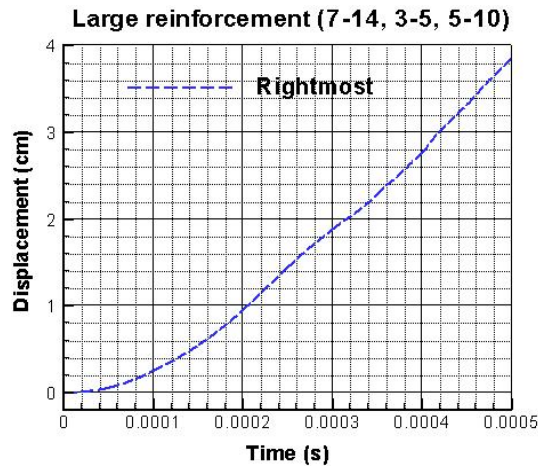


Figure 9 Time-dependent displacement record of the case with retrofitting material structure of $(p, q) = (3, 5), (5, 10)$ and $(7, 14)$.

ACKNOWLEDGEMENT

This work was partially supported by the funding received under a subcontract from the Department of Homeland Security-sponsored Southeast Region Research Initiative (SERRI) at the Department of Energy's Oak Ridge National Laboratory, USA. Authors wish to acknowledge the partial support for this research by ONR Grant# N00014-07-1-1010, Office of Naval Research, Solid Mechanics Program (Dr. Yapa D.S. Rajapakse, Program Manager).

REFERENCES

1. Meguro, M. and Tagel-Din, H. 2000. "Applied element method for structural analysis: theory and application for linear materials," *Structural Eng./Earthquake Eng., JSCE*, **17**(1): 1-14.
2. Oñate, E., Idelsohn, S.R., Pin, F. D, and Aubry., R. 2004. "The particle finite element method. An Overview," *International Journal Computational Method*, **1**(2): 267-307.
3. Monaghan, J. 2005. "Smoothed particle hydrodynamics," *Rep. Prog. Phys.*, **68**(1): 1703-1759.
4. Greenspan, D. 1997. "Particle Modeling," Birkhäuser Publishing.
5. Greenspan, D. 1981. "Computer-Oriented Mathematical Physics," University of Texas at Arlington, Pergamon Press.
6. Wang, G. and Ostoja-Starzewski, M. 2005. "Particle modeling of dynamic fragmentation – I: theoretical considerations," *Computational Materials Science*, **33**: 429-442.
7. Ashby, M.F. and Jones, D.R.H. 1980. "Engineering Materials 1: An Introduction to Their Properties and Applications," Pergamon Press.
8. Ostoja-Starzewski, M. 2007. "Microstructural Randomness and Scaling in Mechanics of Materials," in *Modern Mechanics and Mathematics Series*, Chapman & Hall/CRC/Taylor & Francis.
9. Ostoja-Starzewski, M. 2002. "Lattice models in micromechanics," *Appl. Mech. Rev.*, **55**(1): 35-60.
10. Wang, G., Al-Ostaz, A., Cheng, A.H.-D. and Mantena, P.R. 2008. "Particle modeling of a polymeric material (nylon-6, 6) due to the impact of a rigid indenter," *Computational Materials Science* (in press).
11. Hockney, R.W. and Eastwood, J.W. 1999. "Computer Simulation Using Particles," Institute of Physics Publishing.
12. Wang, G., Radziszewski, P. and Ouellet, J. 2008. "Particle modeling simulation of thermal effects on ore breakage," *Computational Materials Science* (In press).
13. Ostoja-Starzewski, M. and Wang, G. 2006. "Particle modeling of random crack patterns in epoxy plates," *Probabilistic Engineering Mechanics*, **21**: 267-275.
14. Al-Ostaz, A. and Jasiuk, I. 1997. "Crack initiation and propagation in materials with randomly distributed holes," *Engineering Fracture Mechanics*, **58**: 395-420.